

# Correlating the skewness and kurtosis of baryon number distributions

Wei-jie Fu<sup>1</sup> and Jan M. Pawłowski<sup>1,2</sup>

<sup>1</sup>*Institut für Theoretische Physik, Universität Heidelberg, Philosophenweg 16, 69120 Heidelberg, Germany*

<sup>2</sup>*ExtreMe Matter Institute EMMI, GSI, Planckstr. 1, 64291 Darmstadt, Germany*

The skewness and the kurtosis of the baryon number distributions are computed within QCD-improved low energy effective models including quantum thermal and density fluctuations. The results are compared with the Beam Energy Scan experiment at RHIC. The theoretical results agree with the experimental measurements up to errors, for the collision energy  $\sqrt{s} \geq 19.6$  GeV. For smaller collision energies a discrepancy between theoretical and experimental results develops. This discrepancy partially relates to the lack of precision of the current setup for small collision energies. It is outlined how this deficiency can be overcome.

PACS numbers: 11.30.Rd, 11.10.Wx, 05.10.Cc, 12.38.Mh

## I. INTRODUCTION

The evaluation of the QCD phase structure has always been one of the central scientific goals in the community of relativistic heavy ion physics [1]. Large advances have been made in the past years, both from experimental measurements at the Relativistic Heavy-Ion Collider (RHIC) and the Large Hadron Collider (LHC), and theoretical calculations made in various *ab initio* and effective model approaches. The QCD phase diagram is, however, far from being unveiled. One of the most challenging tasks concerning the phase structure of QCD is to access the existence and location of the critical endpoint (CEP) in the phase diagram. If present, it separates the chiral and confinement-deconfinement crossovers at low density from the first order transition at high density, for an overview see [2]. The Beam Energy Scan (BES) program at RHIC is aimed at searching for the CEP of QCD, by employing the beam energy or collision centrality dependence of the fluctuations of conserved charges, e.g. moments of net-proton or net-charge multiplicity distributions [3, 4].

In response to experimental measurements, reliable theoretical predictions of the fluctuations and correlations of conserved charges, as well as their relation to the CEP, are highly demanded. First principles continuum and lattice QCD calculations have made remarkable progress in this direction in recent years, see e.g. [5] and [6]. At present, however, lattice calculations are restricted to the small density regime because of the notorious sign problem, while continuum computation have to deal with the systematics of relevant degrees of freedom at large densities, see e.g. [5].

Recently in [7], we have investigated the QCD thermodynamics and baryon number fluctuations within the framework of QCD-improved low energy effective models, for related work see also [8–20]. Quantum, thermal, and density fluctuations are embedded with the functional renormalization group (FRG) approach to QCD, for recent developments see e.g. [5, 21–26] and references therein.

The computation of baryon number fluctuations neces-

itates a good quantitative grip on the quantum, thermal, and in particular density, fluctuations of the theory. In [7], we therefore have improved the fluctuation analysis beyond former works by including the momentum scale dependence of the quark-meson scattering and the nontrivial dispersions of both quarks and mesons. It was found that the thermodynamics, e.g. the pressure and trace anomaly, and the higher moments of baryon number distributions, after this improvement, agree very well with the lattice results for temperatures  $T \lesssim 1.2 T_c$ . Above these temperatures the ultraviolet limitations of the effective theory setup restrict the applicability, for a detailed discussion see [7]. In this paper, we extend our calculations to finite density, that allows a comparison to the BES experiment at RHIC for given collision energies  $\sqrt{s}$ . For smaller collision energies,  $\sqrt{s} \lesssim 19.6$  GeV, that is larger densities, similar ultraviolet limitations as for large temperatures apply. The current effective theory setup can be systematically improved towards QCD, e.g. [5], which then allows us to go to even smaller collision energies. This is investigated in future work.

## II. EFFECTIVE THEORY SETUP

The present effective theory is embedded in QCD within the functional renormalization group approach. In the present context this is described in detail in [7]. Here we give a brief summary. The flow equation for the scale-dependent effective action of QCD,  $\Gamma_k[\Phi]$ , with the super-field  $\Phi = (A_\mu, c, \bar{c}, q, \bar{q}, \phi, \dots)$  with  $\phi = (\sigma, \vec{\pi})$  and possible further effective hadronic fields, is given by

$$\partial_t \Gamma_k[\Phi] = \frac{1}{2} \text{Tr} G_{\Phi\Phi}[\Phi] \partial_t R_k^\Phi, \quad t = \ln(k/\Lambda), \quad (1)$$

with the full field-dependent propagator,

$$G_{\Phi_i\Phi_j}[\Phi] = \left( \frac{1}{\frac{\delta^2 \Gamma_k[\Phi]}{\delta \Phi^2} + R_k^\Phi} \right)_{ij}. \quad (2)$$

Here  $k$  is the infrared cutoff scale, and  $\Lambda$  is some reference scale, typically the initial UV-scale. The flow equation



FIG. 1. Flow equation for the effective action  $\Gamma$  in full QCD. The four loops correspond to contributions from gluons, ghosts, quarks, and mesons, respectively.

(1) is depicted schematically in Fig. 1, for more details and QCD results, see e.g. [5, 25, 26]. Consequently, the effective action can be written as

$$\Gamma_k[\Phi] = \Gamma_{\text{glue},k}[\Phi] + \Gamma_{\text{matt},k}[\Phi], \quad \Gamma_{\text{matt},k} = \Gamma_{q,k} + \Gamma_{\phi,k}, \quad (3)$$

where  $\Gamma_{\text{glue},k}$  stems from the first two diagrams in Fig. 1, and encodes the ghost- and gluon fluctuations, while  $\Gamma_{q,k}[\Phi]$  stems from the quark loop, and  $\Gamma_{\phi,k}[\Phi]$  from that of the hadronic degrees of freedom. The split in quark and hadronic contributions, within the framework of dynamical hadronization [27–30], is a very efficient parametrization of matter fluctuations in *ab initio* QCD in terms of genuine quark scatterings and resonant momentum channels with hadronic quantum numbers, for applications to QCD see e.g. [25, 26].

Integrating the QCD-flow down to scales  $k = \Lambda$  with  $\Lambda \lesssim 1$  GeV, glue and ghost fluctuations start to decouple from the matter part. This leaves us with an effective matter theory within a glue background. These are the Polyakov-loop-extended chiral models, such as the Polyakov–Nambu–Jona-Lasinio model [31–33] and the Polyakov–quark-meson (PQM) model [34]. In the current extended approximation to the PQM model setup in [7], the matter sector in (3) is given by

$$\Gamma_{\text{matt},k} = \int_x \left\{ Z_{q,k} \bar{q} [\gamma_\mu \partial_\mu - \gamma_0 (\mu + ig A_0)] q + \frac{1}{2} Z_{\phi,k} (\partial_\mu \phi)^2 + h_k \bar{q} \left( T^0 \sigma + i \gamma_5 \vec{T} \cdot \vec{\pi} \right) q + V_k(\rho) - c\sigma \right\}, \quad (4)$$

with  $\int_x = \int_0^{1/T} dx_0 \int d^3x$ . At finite temperatures and for constant gluonic backgrounds, only the temporal component of the gauge field admits a nonvanishing expectation value. The meson field  $\phi = (\sigma, \vec{\pi})$  is in the  $O(4)$  representation, with  $\rho = \phi^2/2$ . The chemical potential  $\mu$  is that of the quark.  $\vec{T}$  are the  $SU(N_f)$  generators with  $\text{Tr}(T^i T^j) = \frac{1}{2} \delta^{ij}$  and  $T^0 = \frac{1}{\sqrt{2N_f}} \mathbb{1}_{N_f \times N_f}$ . The effective potential  $V_k(\rho)$  is  $O(4)$  invariant, and the linear term  $-c\sigma$  breaks the chiral symmetry explicitly.

From (4) and its flow equation (1) we extract flow equations for the effective potential  $V_k(\rho)$ , the Yukawa coupling  $h_k$  as well as the anomalous dimensions of quark and mesonic fields, for details see [7].

As we have discussed above, for renormalization scales  $k \lesssim 1$  GeV, the gluon fluctuations start to decouple from

the matter fluctuations. Hence,  $\Gamma_{\text{glue}}$  in (3) can be expressed as a functional of the gluonic background field. Usually, it is formulated with the expectation value of the traced Polyakov loop, viz.

$$L(\vec{x}) = \frac{1}{N_c} \langle \text{Tr } \mathcal{P}(\vec{x}) \rangle, \quad \text{and} \quad \bar{L} = \frac{1}{N_c} \langle \text{Tr } \mathcal{P}^\dagger(\vec{x}) \rangle, \quad (5)$$

with

$$\mathcal{P}(\vec{x}) = \mathcal{P} \exp \left( ig \int_0^\beta d\tau A_0(\vec{x}, \tau) \right). \quad (6)$$

Hence,  $\Gamma_{\text{glue}}$  relates to the Polyakov loop potential. In this work we adopt the QCD-enhanced glue potential, [21, 22], that is also used in [7]. The QCD enhancement of the potential provides the correct temperature scaling of the glue potential in QCD. QCD-enhanced computations of thermodynamical quantities, i.e. pressure and trace anomaly, agree remarkably well with recent results from lattice QCD for the  $N_f = 2 + 1$  flavor case, see [22].

Apart from the glue potential, we need to specify the initial conditions of the flow equations for the matter sector. We choose the UV-cutoff scale to be  $\Lambda = 700$  MeV in order to maximize the glue decoupling while still keeping as many matter fluctuations as possible, see [7]. The effective potential at this initial scale is well approximated by a classical one, which reads

$$\bar{V}_\Lambda(\bar{\rho}) = \frac{\bar{\lambda}_\Lambda}{2} \bar{\rho}^2 + \bar{\nu}_\Lambda \bar{\rho}, \quad (7)$$

Additionally, we have to specify the Yukawa coupling  $\bar{h}_\Lambda$  and  $\bar{c}_\Lambda$  which sets the amount of explicit chiral symmetry breaking. These relevant couplings are fixed by fitting hadronic observables in the vacuum, the  $\pi$  decay constant  $f_\pi = 92.5$  MeV, the  $\pi$ -meson mass  $m_\pi = 135$  MeV, the  $\sigma$ -meson mass  $m_\sigma = 450$  MeV, and the quark mass  $m_q = 297$  MeV. The obtained values of these couplings are  $\bar{\lambda}_\Lambda = 9.7$ ,  $\bar{\nu}_\Lambda = (0.559 \text{ GeV})^2$ ,  $\bar{h}_\Lambda = 7.2$ ,  $\bar{c}_\Lambda = 1.96 \times 10^{-3} \text{ GeV}^3$ . Note, that in comparison with our former calculations [7] where  $\bar{\nu}_\Lambda$  in (7) is chosen to be vanishing, in this work we exploit the degree of freedom  $\bar{\nu}_\Lambda$  to decrease meson fluctuations above the scale of the chiral symmetry breaking [25, 26]. In the same time, the updated initial conditions reduces the mass of  $\sigma$ -meson to 450 MeV, which is consistent with 400 – 550 MeV of the mass range for  $f_0(500)$  in PDG[35]. We note that a much more restricted range  $446 \pm 6$  MeV of  $f_0(500)$  is also provided, for details, see [35] and reference therein.

Indeed, it has been found in [7] that the thermodynamics at vanishing chemical potential, such as the pressure, trace anomaly, baryon number fluctuations etc., obtained from FRG-calculations, agree very well with the lattice results. With the present improved choice of initial conditions this agreement is even better for large temperature, as expected.

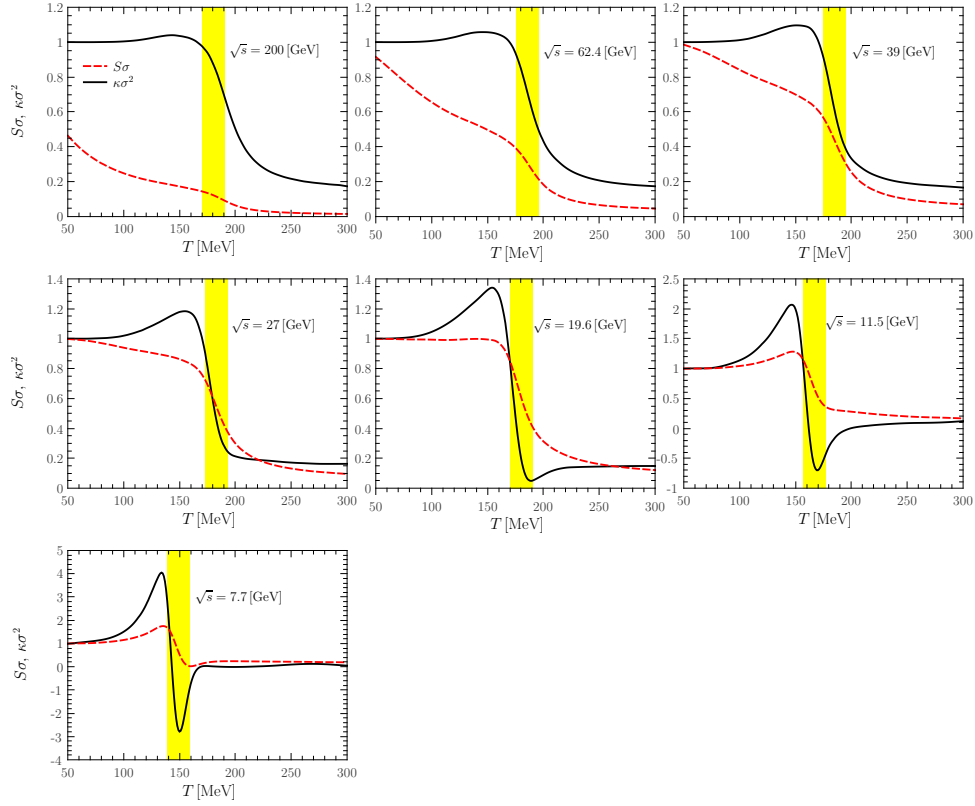


FIG. 2. Skewness  $S\sigma$  (red dashed lines) and kurtosis  $\kappa\sigma^2$  (black solid lines) of the baryon number distributions as functions of the temperature, for different values of chemical potential, i.e. different collision energy, shown in Table I. The yellow vertical band in each plot shows an estimate of the freeze-out temperature, with its center located at a temperature which produces the measured  $S\sigma$  in experiments. All bands have a width of 20 MeV accounting for the systematic errors, for details see the discussion below (11).

### III. SKEWNESS AND KURTOSIS OF THE BARYON NUMBER DISTRIBUTION

The baryon number fluctuations are given by

$$\chi_n^B = \frac{\partial^n}{\partial(\mu_B/T)^n} \frac{p}{T^4}, \quad (8)$$

with the pressure  $p = -(\Gamma_{k=0,T}[\Phi] - \Gamma_{k=0,T=0}[\Phi])$  and baryon number chemical potential  $\mu_B = 3\mu$ . The  $\chi_n^B$  are related to the cumulants of baryon multiplicity distributions: for example, the mean value  $M$  is given by  $M = VT^3\chi_1^B$ , the variance is  $\sigma^2 = VT^3\chi_2^B$ , the skewness is  $S = \chi_3^B/(\chi_2^B\sigma)$ , and the kurtosis is  $\kappa = \chi_4^B/(\chi_2^B\sigma^2)$ . Here  $V$  is the volume of the system.  $S\sigma$  and  $\kappa\sigma^2$  are the volume-independent skewness and kurtosis, respectively.

In order to compare our calculated results with experiments we need the chemical freeze-out line, the freeze-out chemical potential and temperature in terms of the collision energy  $\sqrt{s}$ . We employ the freeze-out line in [36, 37], consistent with that in [38]. For more discussions about the freeze-out conditions, see e.g. [39–41]. For the experimental comparison, we have to rescale the chemical potential and temperature in the present  $N_f = 2$  computations, in order to take care of the different absolute

scales. The relationship between the absolute temperature scale in  $N_f = 2$  flavor and that in  $N_f = 2 + 1$ , as demonstrated in [7, 22], suggests to adopt the following linear rescaling for the chemical potential,

$$\mu_{B,N_f=2} = \beta \mu_{B,N_f=2+1}, \quad (9)$$

with the parameter  $\beta \geq 1$ . The absolute scale of the chemical potential is gauged by  $\mu_c$ , the chemical potential of the liquid gas transition, which is closely related to the mass scales of the theory. This seemingly suggests  $\beta = 1$ , as the meson and quark mass scales are fixed to their physical value in the vacuum. Note that the mass parameters in the model are curvature masses, and the mass adjustment applies to the pole masses, see [24, 42, 43]. It has been shown in [24] that the latter agree relatively well for the mesons, but might differ for the quarks. In turn,  $\beta > 1$  is suggested by the relation of the critical temperatures.

Here we determine  $\beta$  as follows: for each collision energy and given  $\beta$  we employ the experimentally measured skewness  $S\sigma = \chi_3^B/\chi_2^B$  and the  $\sigma^2/M = \chi_2^B/\chi_1^B$  in [4] to determine the freeze-out temperatures, denoted by  $T_f(\chi_3^B/\chi_2^B)$  and  $T_f(\chi_2^B/\chi_1^B)$ , respectively. For general  $\beta$  these two freeze-out temperatures differ. In the follow-

| $\sqrt{s}$ [GeV]               | 200  | 62.4 | 39  | 27    | 19.6  | 11.5 | 7.7   |
|--------------------------------|------|------|-----|-------|-------|------|-------|
| $\mu_{B,N_f=2}$ [MeV]          | 25.3 | 78.1 | 121 | 168.7 | 222.7 | 343  | 459.4 |
| $T_f(\chi_3^B/\chi_2^B)$ [MeV] | 180  | 186  | 185 | 183   | 180   | 167  | 149   |
| $T_f(\chi_2^B/\chi_1^B)$ [MeV] | 178  | 183  | 188 | 182   | 178   | 168  | 154   |

TABLE I.  $\mu_{B,N_f=2}$ ,  $T_f(\chi_3^B/\chi_2^B)$  and  $T_f(\chi_2^B/\chi_1^B)$  corresponding to different collision energy, with  $\beta = 1.13$  in Eq. (9). Here, we have employed the data of  $S\sigma$  and  $\sigma^2/M$  measured in Au + Au collisions at RHIC with centrality 0 – 5%, for details see [4].

ing we fix a constant  $\beta$  by the requirement

$$T_f(\chi_3^B/\chi_2^B) \approx T_f(\chi_2^B/\chi_1^B), \quad (10)$$

for all collision energies. With this requirement, we obtain  $\beta = 1.13$ . In Tab. I we present the relevant  $\mu_{B,N_f=2}$ ,  $T_f(\chi_3^B/\chi_2^B)$  and  $T_f(\chi_2^B/\chi_1^B)$ . The slight variations of about 5 MeV for the two freeze-out temperatures relate to the constant choice of  $\beta$ . We emphasize, that this has little impact on the current results. Note also that the freeze-out curve in the present approach with its additional constraints on the freeze-out temperature is consistent with the results in [36, 37] after an appropriate rescaling.

We also note that  $\beta = 1.13$  is close to the  $\beta$  which one gets from simply taking over the relation of the absolute temperature scales, to wit,

$$\mu_{B,N_f=2} = \frac{T_{c,N_f=2}}{T_{c,N_f=2+1}} \mu_{B,N_f=2+1}, \quad (11)$$

where  $T_{c,N_f=2} = 180$  MeV is the pseudocritical temperature at  $\mu_B = 0$  for  $N_f = 2$ , and  $T_{c,N_f=2+1} = 155$  MeV is the pseudocritical temperature at  $\mu_B = 0$  for  $N_f = 2 + 1$  lattice simulations [44]. The latter also agrees with the freeze-out temperature [38]. Substituting these values into (11), one finds  $\beta = 1.16$ .

We proceed by discussing the systematic error in our temperature estimate. First of all,  $T_f(\chi_3^B/\chi_2^B)$  and  $T_f(\chi_2^B/\chi_1^B)$  do not have to agree precisely, and only provide estimates for the freeze-out temperature. The latter one also has a bigger uncertainty, but in most regimes they differ by less than 10 MeV in an appropriate  $\beta$ -range. We conclude that 20 MeV accounts well for the related systematic error leading to the yellow error bands in Fig. 2.

#### IV. RESULTS

To begin with, we note that the chemical potential of electric charge  $\mu_Q$  has been shown to be quite small in comparison to  $\mu_B$  [8], and hence is neglected in our calculations. Furthermore, the experiments measure the moments of net-proton multiplicity distributions. Note, that yet there has not been a conclusive answer about the relation between the net-baryon number and the net-proton number fluctuations. It was demonstrated in [45]

that the difference between them is small, if the Boltzmann approximation for the baryon distribution is only violated mildly. However, it is generally believed that in more realistic heavy-ion collisions the situation is more complicated, see e.g. [46, 47]. Then, because of the global baryon number conservation, the net-baryon number and the net-proton number fluctuations are affected differently [48, 49]. In this work we neglect these intricacies for the sake of simplicity.

In Fig. 2 we show the skewness and the kurtosis of baryon number distributions as functions of temperature for different values of the collision energy  $\sqrt{s}$ . Different collision energy relates to different chemical potentials, see Table I. Note that the QGP produced in heavy-ion collisions evolves with time, and the nonequilibrium skewness and kurtosis might differ from equilibrium expectations, see e.g. [50]. For more discussions about the dynamical evolution of fluctuations, see e.g. [51–53]. Thus, it is expected that a range of  $T$  near the freeze-out temperature, rather than a single value, affects experimental measurements.

Note also that fixing the freeze-out temperature with different fluctuation observables does not necessarily result in identical results, though we have checked for  $S\sigma$  and  $\sigma^2/M$  that the differences are small, see Tab. I. Finally, a variation of the parameters (initial conditions) of the present low energy effective theory can be used to effectively slightly shift the skewness and kurtosis curves relative to each other. The ensuing systematic error has been discussed below (11), and leads to a loss of predictive power below 15-20 GeV collision energy, signalled by the vertical line in Fig. 3: for decreasing collision energy the transition strength of the crossover becomes larger. Then the amplitude of fluctuations, especially the kurtosis  $\kappa\sigma^2$ , increases as well, as does the systematic error. Nonetheless, it is remarkable that for collision energy less than 19.6 GeV, the kurtosis  $\kappa\sigma^2$  gets negative in a regime, which roughly overlaps with the yellow band.

In Fig. 3 our results for  $S\sigma$  and  $\kappa\sigma^2$  are compared with experimental results by the STAR Collaboration at RHIC. The shaded area in Fig. 3 provides our systematic error estimate, which covers the variation ranges of  $\kappa\sigma^2$  within the yellow bands in Fig. 2. Moreover, for the collision energies  $\sqrt{s} < 19.6$  GeV, the related freeze-out chemical potentials are bigger than 300 MeV, and hence are of the order of the UV cutoff scale  $\Lambda$ . Following [24], we investigate the UV limitations of the present effective theory setup: if the flow shows strong deviations from the vacuum flow at the initial scale for large  $T$  and  $\mu_B$ , a significant part of the fluctuations is not encoded within the flow. Note also, that enlarging  $\Lambda$  brings us into the regime, where glue quantum fluctuations become increasingly important. Hence, a larger UV cutoff scale does not resolve the problem. The black vertical lines in Fig. 3 show the collision energy  $\sqrt{s} \sim 15.6$  GeV, corresponding to  $\mu_B \sim 270$  MeV, below which the UV-cutoff effects become obvious. In other words, when the chemical potential is larger than  $\sim 270$  MeV, quantum fluctuations

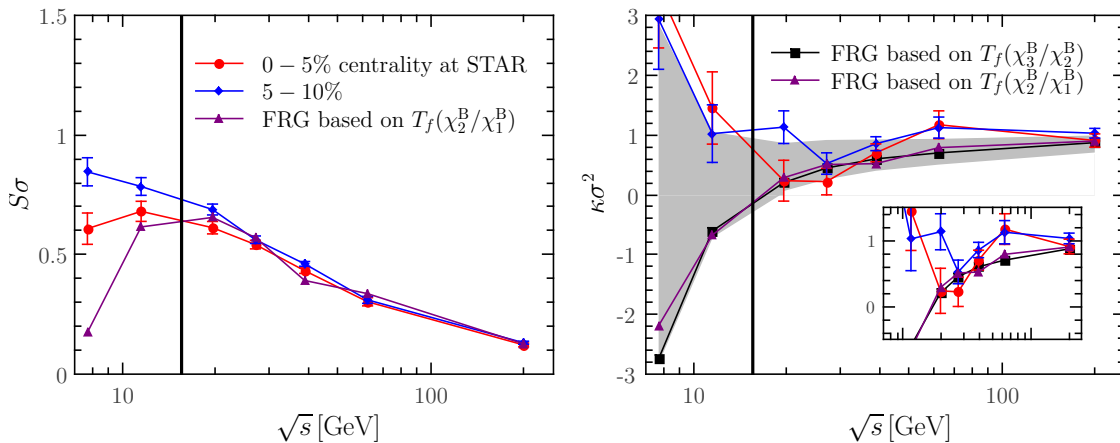


FIG. 3. Theoretical calculations of  $S\sigma$  (left panel) and  $\kappa\sigma^2$  (right panel) as functions of the collision energy, in comparison with experimental measurements in Au + Au collisions at RHIC with centralities 0 – 5%, 5 – 10% [4]. The gray regions show error estimates resulting from the determination of freeze-out temperatures, which corresponds to the vertical yellow bands in Fig. 2. The black vertical lines indicate the collision energy, below which the UV-cutoff effect becomes significant.

of mesons above the scale of the UV-cutoff are not negligible any more, and thus our current setup has to be improved with QCD-fluctuations. This is deferred to future work.

Finally, finite volume effects [19], volume fluctuations [54] and the difference between the net-proton and net-baryon number fluctuations due to, e.g. the effect of global baryon number conservation [48], should be also considered in a full analysis of small collision energies.

Recently, [4], the transverse momentum ( $p_T$ ) acceptance has been extended from  $0.4 < p_T < 0.8$  GeV/ $c$  in the first release of experimental data in [3] to  $0.4 < p_T < 2$  GeV/ $c$ . Here, we compare our calculations with the updated  $S\sigma$  and  $\kappa\sigma^2$  of net-proton distributions in Au + Au collisions with centralities 0% – 5%, 5% – 10%, and rapidity  $|y| < 0.5$  [4]. These are consistent with recent findings that larger rapidity and  $p_T$  acceptance results in a significantly larger critical point signal [55].

First of all, we employ the freeze-out temperature  $T_f(\chi_3^B/\chi_2^B)$  in Tab. I, which is determined by the experimentally measured  $S\sigma$ , i.e. the red circular points in the left panel of Fig. 3. Then one can compare the computed kurtosis  $\kappa\sigma^2$  with the experimental results, as shown by the black squares in the right panel. We find, that for collision energies  $\sqrt{s} \geq 19.6$  GeV our  $\kappa\sigma^2$  agrees with the experimental measurements within the error bars. For collision energies below 19.6 GeV, the theoretical  $\kappa\sigma^2$  drops rapidly and changes sign with the decrease of the energy. In turn, the experimental value of  $\kappa\sigma^2$  rises, as also shown in the inlay plot of Fig. 3. Then, we use  $T_f(\chi_2^B/\chi_1^B)$  as the freeze-out temperature in lieu of  $T_f(\chi_3^B/\chi_2^B)$ , and the relevant  $S\sigma$  and  $\kappa\sigma^2$  are presented in Fig. 3 by triangles. This provides another systematic error check of the present computations. We find that the results of  $S\sigma$  based on  $T_f(\chi_2^B/\chi_1^B)$  start to deviate significantly from the experimental results for collision energies  $\sqrt{s} < 19.6$  GeV. In contradistinction,

$\kappa\sigma^2$  based on  $T_f(\chi_2^B/\chi_1^B)$  is consistent with that based on  $T_f(\chi_3^B/\chi_2^B)$  for all collision energies. Note however, that this simply originates in the fact that for low collision energy the freeze-out temperatures, both  $T_f(\chi_3^B/\chi_2^B)$  and  $T_f(\chi_2^B/\chi_1^B)$ , are close to those corresponding to the minimum of  $\kappa\sigma^2$ , as shown in Fig. 2. Consequently, theoretical curves in the right panel of Fig. 3 are at the bottom of the error estimates, and are not trustworthy anymore.

## V. SUMMARY AND CONCLUSIONS

The skewness and kurtosis of baryon number distributions at finite temperature and chemical potential are calculated within a QCD-improved low energy effective theory. The setup includes quantum thermal and density fluctuations within the functional renormalization group approach. The present theoretical results are compared with recent experimental measurements. Given the skewness, our calculated kurtosis agrees with the experimental measurements up to errors, for the collision energy  $\sqrt{s} \geq 19.6$  GeV. For smaller collision energies such a comparison is affected by several intricacies: the experimental data are affected by kinematic cuts, and are only sensitive to the net proton number. Moreover, we have not taken into account the nonequilibrium nature of the heavy ion collision. Furthermore, the present setup has to be improved systematically towards QCD for small collision energies, i.e., pushing the initial scale of UV-cutoff to a regime of perturbative QCD, and including quantum fluctuations of the glue part, for more discussions about the full QCD in the vacuum, see e.g.[5]. This extension is currently under progress.

# ACKNOWLEDGMENTS

We thank X. Luo for providing us with the experimental data, and T. K. Herbst, M. Mitter, F. Rennecke, B.-J.

Schaefer, N. Strodthoff for valuable discussions and work on related subjects. W.-J. Fu thanks also the support of Alexander von Humboldt Foundation. This work is supported by EMMI, and by ERC-AdG-290623.

- 
- [1] Y. Akiba *et al.*, (2015), arXiv:1502.02730 [nucl-ex].
  - [2] M. Stephanov, PoS **LAT2006**, 024 (2006), arXiv:hep-lat/0701002 [hep-lat].
  - [3] L. Adamczyk *et al.* (STAR), Phys.Rev.Lett. **112**, 032302 (2014), arXiv:1309.5681 [nucl-ex].
  - [4] X. Luo (STAR), *9th International Workshop on Critical Point and Onset of Deconfinement (CPOD 2014) Bielefeld, Germany, November 17-21, 2014*, PoS **CPOD2014**, 019 (2014), arXiv:1503.02558 [nucl-ex].
  - [5] J. M. Pawłowski, Nucl.Phys. **A931**, 113 (2014).
  - [6] G. Aarts (2015) arXiv:1512.05145 [hep-lat].
  - [7] W.-j. Fu and J. M. Pawłowski, Phys. Rev. **D92**, 116006 (2015), arXiv:1508.06504 [hep-ph].
  - [8] S. Borsanyi, Z. Fodor, S. Katz, S. Krieg, C. Ratti, *et al.*, Phys.Rev.Lett. **111**, 062005 (2013), arXiv:1305.5161 [hep-lat].
  - [9] H.-T. Ding, *Proceedings, 24th International Conference on Ultra-Relativistic Nucleus-Nucleus Collisions (Quark Matter 2014)*, Nucl. Phys. **A931**, 52 (2014), arXiv:1408.5236 [hep-lat].
  - [10] V. Skokov, B. Stokic, B. Friman, and K. Redlich, Phys.Rev. **C82**, 015206 (2010), arXiv:1004.2665 [hep-ph].
  - [11] V. Skokov, B. Friman, E. Nakano, K. Redlich, and B.-J. Schaefer, Phys.Rev. **D82**, 034029 (2010), arXiv:1005.3166 [hep-ph].
  - [12] V. Skokov, B. Friman, and K. Redlich, Phys.Rev. **C83**, 054904 (2011), arXiv:1008.4570 [hep-ph].
  - [13] F. Karsch, B.-J. Schaefer, M. Wagner, and J. Wambach, Phys.Lett. **B698**, 256 (2011), arXiv:1009.5211 [hep-ph].
  - [14] B. J. Schaefer and M. Wagner, Phys. Rev. **D85**, 034027 (2012), arXiv:1111.6871 [hep-ph].
  - [15] B.-J. Schaefer and M. Wagner, Central Eur.J.Phys. **10**, 1326 (2012), arXiv:1203.1883 [hep-ph].
  - [16] K. Morita, B. Friman, and K. Redlich, Phys. Lett. **B741**, 178 (2015), arXiv:1402.5982 [hep-ph].
  - [17] K. Morita and K. Redlich, PTEP **2015**, 043D03 (2015), arXiv:1409.8001 [hep-ph].
  - [18] X.-y. Xin, S.-x. Qin, and Y.-x. Liu, Phys. Rev. **D90**, 076006 (2014).
  - [19] J. Chen, F. Gao, and Y.-x. Liu, (2015), arXiv:1510.07543 [hep-ph].
  - [20] G. A. Almsi, B. Friman, and K. Redlich, in *25th International Conference on Ultra-Relativistic Nucleus-Nucleus Collisions (Quark Matter 2015) Kobe, Japan, September 27-October 3, 2015* (2016) arXiv:1601.00782 [hep-ph].
  - [21] L. M. Haas, R. Stiele, J. Braun, J. M. Pawłowski, and J. Schaffner-Bielich, Phys.Rev. **D87**, 076004 (2013), arXiv:1302.1993 [hep-ph].
  - [22] T. K. Herbst, M. Mitter, J. M. Pawłowski, B.-J. Schaefer, and R. Stiele, Phys.Lett. **B731**, 248 (2014), arXiv:1308.3621 [hep-ph].
  - [23] J. M. Pawłowski and F. Rennecke, Phys. Rev. D **90**, 076002 (2014), arXiv:1403.1179 [hep-ph].
  - [24] A. J. Helmboldt, J. M. Pawłowski, and N. Strodthoff, Phys.Rev. **D91**, 054010 (2015), arXiv:1409.8414 [hep-ph].
  - [25] M. Mitter, J. M. Pawłowski, and N. Strodthoff, Phys.Rev. **D91**, 054035 (2015), arXiv:1411.7978 [hep-ph].
  - [26] J. Braun, L. Fister, J. M. Pawłowski, and F. Rennecke, (2014), arXiv:1412.1045 [hep-ph].
  - [27] H. Gies and C. Wetterich, Phys.Rev. **D65**, 065001 (2002), arXiv:hep-th/0107221 [hep-th].
  - [28] H. Gies and C. Wetterich, Phys.Rev. **D69**, 025001 (2004), arXiv:hep-th/0209183 [hep-th].
  - [29] J. M. Pawłowski, Annals Phys. **322**, 2831 (2007), arXiv:hep-th/0512261 [hep-th].
  - [30] S. Floerchinger and C. Wetterich, Phys.Lett. **B680**, 371 (2009), arXiv:0905.0915 [hep-th].
  - [31] K. Fukushima, Phys.Lett. **B591**, 277 (2004), arXiv:hep-ph/0310121 [hep-ph].
  - [32] C. Ratti, M. A. Thaler, and W. Weise, Phys.Rev. **D73**, 014019 (2006), arXiv:hep-ph/0506234 [hep-ph].
  - [33] W.-j. Fu, Z. Zhang, and Y.-x. Liu, Phys.Rev. **D77**, 014006 (2008), arXiv:0711.0154 [hep-ph].
  - [34] B.-J. Schaefer, J. M. Pawłowski, and J. Wambach, Phys.Rev. **D76**, 074023 (2007), arXiv:0704.3234 [hep-ph].
  - [35] K. Olive *et al.* (Particle Data Group), Chin.Phys. **C38**, 090001 (2014).
  - [36] A. Andronic, P. Braun-Munzinger, and J. Stachel, Nucl. Phys. **A772**, 167 (2006), arXiv:nucl-th/0511071 [nucl-th].
  - [37] A. Andronic, P. Braun-Munzinger, and J. Stachel, Phys. Lett. **B673**, 142 (2009), [Erratum: Phys. Lett.B678,516(2009)], arXiv:0812.1186 [nucl-th].
  - [38] S. Borsanyi, Z. Fodor, S. D. Katz, S. Krieg, C. Ratti, and K. K. Szabo, Phys. Rev. Lett. **113**, 052301 (2014), arXiv:1403.4576 [hep-lat].
  - [39] A. Bazavov *et al.*, Phys. Rev. Lett. **109**, 192302 (2012), arXiv:1208.1220 [hep-lat].
  - [40] F. Karsch and K. Redlich, Phys. Lett. **B695**, 136 (2011), arXiv:1007.2581 [hep-ph].
  - [41] P. Alba, W. Alberico, R. Bellwied, M. Bluhm, V. Mantovani Sarti, M. Nahrgang, and C. Ratti, Phys. Lett. **B738**, 305 (2014), arXiv:1403.4903 [hep-ph].
  - [42] N. Strodthoff, B.-J. Schaefer, and L. von Smekal, Phys.Rev. **D85**, 074007 (2012), arXiv:1112.5401 [hep-ph].
  - [43] R.-A. Tripolt, N. Strodthoff, L. von Smekal, and J. Wambach, Phys.Rev. **D89**, 034010 (2014), arXiv:1311.0630 [hep-ph].
  - [44] S. Borsanyi *et al.* (Wuppertal-Budapest Collaboration), JHEP **1009**, 073 (2010), arXiv:1005.3508 [hep-lat].
  - [45] K. Fukushima, Phys. Rev. **C91**, 044910 (2015), arXiv:1409.0698 [hep-ph].
  - [46] M. Kitazawa and M. Asakawa, Phys. Rev. **C85**, 021901 (2012), arXiv:1107.2755 [nucl-th].

- [47] M. Kitazawa and M. Asakawa, Phys. Rev. **C86**, 024904 (2012), [Erratum: Phys. Rev.C86,069902(2012)], arXiv:1205.3292 [nucl-th].
- [48] M. Nahrgang, T. Schuster, M. Mitrovski, R. Stock, and M. Bleicher, Eur. Phys. J. **C72**, 2143 (2012), arXiv:0903.2911 [hep-ph].
- [49] A. Bzdak, V. Koch, and V. Skokov, Phys. Rev. **C87**, 014901 (2013), arXiv:1203.4529 [hep-ph].
- [50] S. Mukherjee, R. Venugopalan, and Y. Yin, Phys. Rev. **C92**, 034912 (2015), arXiv:1506.00645 [hep-ph].
- [51] M. Hippert, E. S. Fraga, and E. M. Santos, Phys. Rev. **D93**, 014029 (2016), [Phys. Rev.D93,014029(2016)], arXiv:1507.04764 [hep-ph].
- [52] L. Jiang, P. Li, and H. Song, (2015), arXiv:1512.06164 [nucl-th].
- [53] C. Herold, M. Nahrgang, Y. Yan, and C. Kobdaj, Phys. Rev. **C93**, 021902 (2016), arXiv:1601.04839 [hep-ph].
- [54] V. Skokov, B. Friman, and K. Redlich, Phys. Rev. **C88**, 034911 (2013), arXiv:1205.4756 [hep-ph].
- [55] B. Ling and M. A. Stephanov, (2015), arXiv:1512.09125 [nucl-th].